# Copper nanocrystal morphology determines the viability of molecular surface functionalization in tuning electrocatalytic behavior in $CO_2$ reduction

James R. Pankhurst, Pranit Iyengar, Valery Okatenko, Raffaella Buonsanti*

Laboratory of Nanochemistry for Energy (LNCE), Institute of Chemical Sciences and Engineering (ISIC), École Polytechnique Fédérale de Lausanne (EPFL), Rue de l'Industrie 17, 1950 Sion, Valais, Switzerland

**ABSTRACT**

Molecular surface functionalization of metallic catalysts is emerging as an ever-developing approach to tune their catalytic performance. Here, we report the synthesis of hybrid catalysts comprising copper nanocrystals (CuNCs) and an imidazolium ligand for the electrochemical $CO_2$ reduction reaction ($CO_2$RR). We show that this organic modifier steers the selectivity of cubic CuNCs towards liquid products. The comparison between cubic and spherical CuNCs reveals the impact of surface reconstruction on the viability of surface functionalization schemes. Indeed, the intrinsic instability of the spherical CuNCs leads to the ejection of the functionalized surface

atoms. Finally, we also demonstrate that the more stable hybrid NC catalysts, which include cubic CuNCs, can be transferred into gas-flow $CO_2$RR cells for testing under more industrially relevant conditions.

## INTRODUCTION

The electrochemical $CO_2$ reduction reaction ($CO_2$RR) has gained intense interest from an array of scientific fields due to its potential to address future energy and environmental demands.[1] By using $CO_2$, water and electrical energy for the synthesis of energy-dense hydrocarbons, the storage of intermittent renewable energy in the form of chemical bonds whilst progressing towards a closed carbon cycle is envisioned.[2,3]

Copper is the only single metal that is known to form C–C bonds during the $CO_2$RR, leading to desirable products such as hydrocarbons and alcohols. However, this catalyst suffers from an intrinsic selectivity problem, as 16 different products form on a polycrystalline foil.[2,3] Studies on single crystals have revealed the structural sensitivity of the reaction, with certain facets being more selective for certain products.[4–7] Because of their capability of translating these findings identified on copper surfaces into more realistic conditions, copper nanocrystals (NCs) have been at the forefront of $CO_2$RR research.[4,5,8–12] For example, cubic CuNCs have attracted particular interest, as the interface between the exposed (100) facets and (110) edge sites has been found to favor C-C coupling towards ethylene.[6,10,13–16]

In addition to such structural modifications, the coupling of pure metal surfaces with organic coatings and ligands has gained increased interest in recent years.[17,18-34] These studies have revealed the huge potential of combining the fields of homogeneous and heterogeneous catalysis to steer selectivity in the $CO_2$RR.[22-34] They have also evidenced that the surface chemistry of modified catalysts is both rich and complex, as many factors that influence catalysis are at play.[19–22] Ligands can steer the reaction mechanism towards single products by influencing the binding energies of specific intermediates, either by modification of the properties of the metal itself[23–25], or by direct interaction with intermediates at the surface[26–29]. Ligands can also influence the interface between the metal and the reaction medium, altering reactant concentration profiles[30], or even establishing new phase boundaries[31,32]. However, not much attention has been dedicated so far to the link between the metal catalyst reconstruction during operation and the effects induced by the organic modifiers.

In this work we illustrate how the stability of the NC catalyst is crucial in allowing the effects of surface ligands to emerge. Specifically, we study CuNCs functionalized with a disubstituted imidazolium ligand (1-octyl-3-(*para*-nitrobenzyl)-imidazolium hexafluorophosphate, **$ImPF_6$**) as $CO_2$RR electrocatalysts. This molecule was selected based on our recent study where we investigated several disubstituted imidazolium ligands as $CO_2$RR promoters on the surfaces of AgNC catalysts.[33] In addition to the interaction of the imidazolium group with $CO_2$, we found that the $C_8$ tail length was optimal to promote the selectivity towards $CO_2$RR versus the competing hydrogen evolution reaction (HER).

In the case of CuNCs, we observe that the selectivity changes towards liquid products at intermediate potentials when functionalized with the imidazolium ligand. More importantly, the

comparison between cubic and spherical CuNCs highlights that morphologically stable NCs must be employed for studying hybrid catalyst systems. Finally, we demonstrate that the imidazolium-functionalized cubic CuNC catalysts can be transferred to gas-flow electrochemical setups for testing under elevated current densities, thus illustrating the eventual suitability of these catalysts for commercial applications.

## RESULTS AND DISCUSSION

We have synthesized cubic CuNCs (**$Cu_{cub}$**) according to our previously reported colloidal synthesis route (**Figure S1**).[10] The native trioctylphosphine oxide (TOPO) ligands were exchanged with the **$ImPF_6$** according to the scheme illustrated in **Figure 1A**.

Solvent washing was used to remove the native TOPO from as-synthesized **$Cu_{cub}$** (**$Cu_{cub}$-TOPO**) before functionalization with the **$ImPF_6$** to form the **$Cu_{cub}$-$ImPF_6$** hybrid catalyst (**Figure 1A**). TEM characterization shows that no sintering or etching of the particles occurred using this procedure (**Figure 1B**). We note that, compared with our previous work on AgNCs, the exchange of the $Br^-$ counter-ion for $PF_6^-$ was necessary as the former induced severe restructuring in the CuNCs (**Figure S2–S4**), which is consistent with other work involving Cu foils.[34]

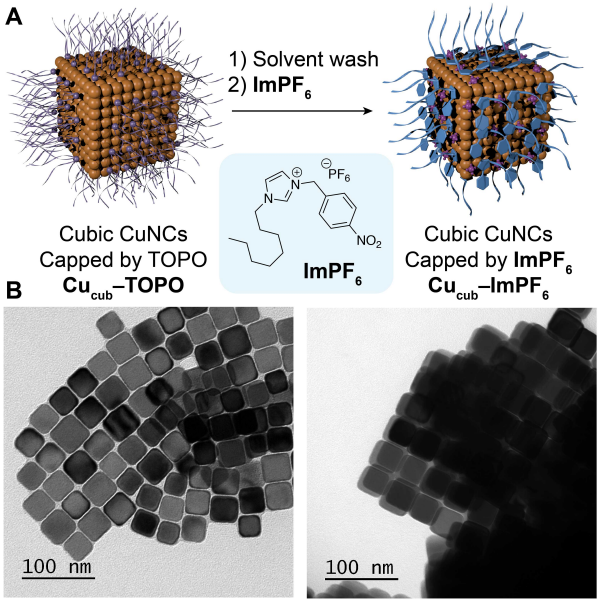


**Figure 1.** A) Overview of the ligand-exchange procedure to obtain imidazolium-functionalized CuNCs (**$Cu_{cub}$-$ImPF_6$**). B) TEM images of as-synthesized **$Cu_{cub}$**, functionalized with TOPO, and of **$Cu_{cub}$-$ImPF_6$**.

Successful ligand exchange on **$Cu_{cub}$** was supported by FT-IR spectroscopy (**Figure 2A**). The strong absorption bands for the **$ImPF_6$** nitro groups are observed at 1517 and 1341 $cm^{-1}$, and the band arising from the $PF_6^-$ stretch is observed at 828 $cm^{-1}$. Absorption bands corresponding to the imidazolium C–H stretches are shifted to lower frequency on the **$Cu_{cub}$** surface, appearing at 3156 $cm^{-1}$ compared to 3164 $cm^{-1}$ for the free ligand. This suggests that **$ImPF_6$** interacts with the Cu surface through the imidazolium ring.

X-ray photoelectron spectroscopy (XPS) confirmed the presence of the **$ImPF_6$** ligands on the **$Cu_{cub}$** surface (**Figures 2B**, **S5**). No peaks were observed in the N1s region for the as-synthesized CuNCs, but after functionalization with **$ImPF_6$**, peaks emerged at 406.1 eV, 401.9 eV and 400.5 eV, corresponding to the $NO_2$ functional group and the two nitrogen atoms in an asymmetric

imidazolium ring. XPS spectra in the O1s region evidenced a large increase in the amount of organic-based oxygen compared with the metal-oxide content, consistent with the introduction of nitro-containing **$ImPF_6$** ligands. Finally, a single peak in the F1s region was observed following functionalization with **$ImPF_6$**, showing the presence of the $PF_6^-$ anion. The electronic structure of the Cu surface was also investigated by XPS, which revealed that the **$ImPF_6$** ligand does not introduce any significant change (**Figure S6**, **Table S1**). The Cu2p photoelectron and Cu LMM Auger spectra were indicative of a mixture of Cu(0) and Cu(I) oxidation states for the **$Cu_{cub}$** surface, both before and after functionalization with **$ImPF_6$**.

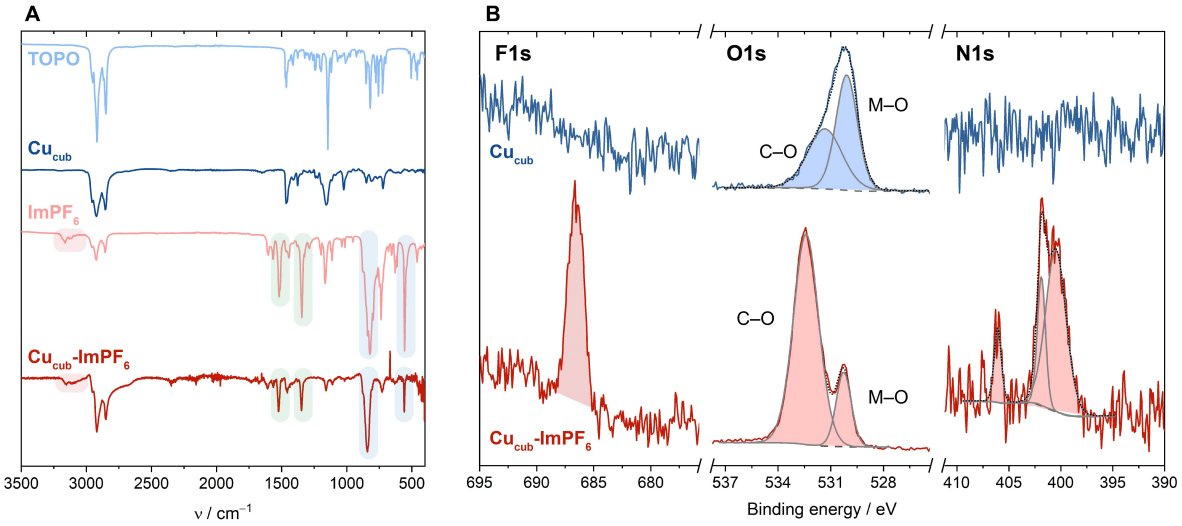


**Figure 2.** A) FT-IR spectra of TOPO, **$Cu_{cub}$**, **$ImPF_6$** and **$Cu_{cub}$-$ImPF_6$**. Absorption bands corresponding to the **$ImPF_6$** imidazolium C–H stretches, nitro N–O stretches and P–F stretches are highlighted in red, green and blue, respectively. B) XPS spectra evidencing the introduction of the **$ImPF_6$** ligand are shown for the F1s, O1s and N1s regions.

The $CO_2$RR performance of the CuNC catalysts was first assessed using a H-cell configuration, where the catalysts were drop-cast on glassy carbon electrodes. Previous studies have shown that optimal $CO_2$RR performance is achieved for cubic CuNCs in 0.1 M $KHCO_3$ at −1.1 $V_{RHE}$,[5,8–12] and the catalysts in this study were therefore tested at a range of potentials around this value (more than 80% hydrogen is generated at potentials more positive than −1.05 $V_{RHE}$). Solvent washing of as-synthesized $\mathbf{Cu_{cub}}$ was carried out after drop-casting to remove the native TOPO ligands so as to provide a naked reference sample. The $\mathbf{Cu_{cub}}$-$\mathbf{ImPF_6}$ catalyst was tested after deposition without any additional solvent washing. In line with previous studies, $\mathbf{Cu_{cub}}$ produced mainly $H_2$ at −1.05 $V_{RHE}$ , then ethylene as the major $CO_2$RR product at −1.10 $V_{RHE}$ with a Faradaic efficiency (F.E.) of 36% and finally methane as the dominant $CO_2$RR product as the potential became more negative, with F.E. of 23% at -1.20 $V_{RHE}$ (**Figure 3A**).[35]

After functionalization with $\mathbf{ImPF_6}$, the overall $CO_2$RR vs HER selectivity remained similar to the pristine $\mathbf{Cu_{cub}}$ at −1.05 and −1.10 $V_{RHE}$, while less $H_2$ was produced at −1.15 and −1.20 $V_{RHE}$. At −1.20 $V_{RHE}$, $FE_{H2}$ was only 24% for $\mathbf{Cu_{cub}}$-$\mathbf{ImPF_6}$ against 40% for $\mathbf{Cu_{cub}}$, indicating a HER suppression effect of the imidazolium ligand at more negative potentials, which is consistent with our previous work.[33] Among the $CO_2$RR products, the CO selectivity was equivalent for both catalysts across the range of potentials. Conversely, ethylene formation was suppressed on the $\mathbf{Cu_{cub}}$-$\mathbf{ImPF_6}$ catalyst at −1.05, −1.10 and −1.15 $V_{RHE}$ (the F.E. is only 22% at −1.10 $V_{RHE}$). Concomitantly, an increase in the liquid products was observed, with formate being the major product (**Figure 3A**). This is seen more clearly when the liquid/gas product ratios are compared across the studied potential range (**Figure 3B**), with the maximum change in selectivity being observed at −1.10 $V_{RHE}$. At the most negative potential of −1.20 $V_{RHE}$, the ethylene and liquid

product selectivities are again similar to those of **$Cu_{cub}$**, as the strongly negative potential still favors methane formation even in the presence of **$ImPF_6$**.

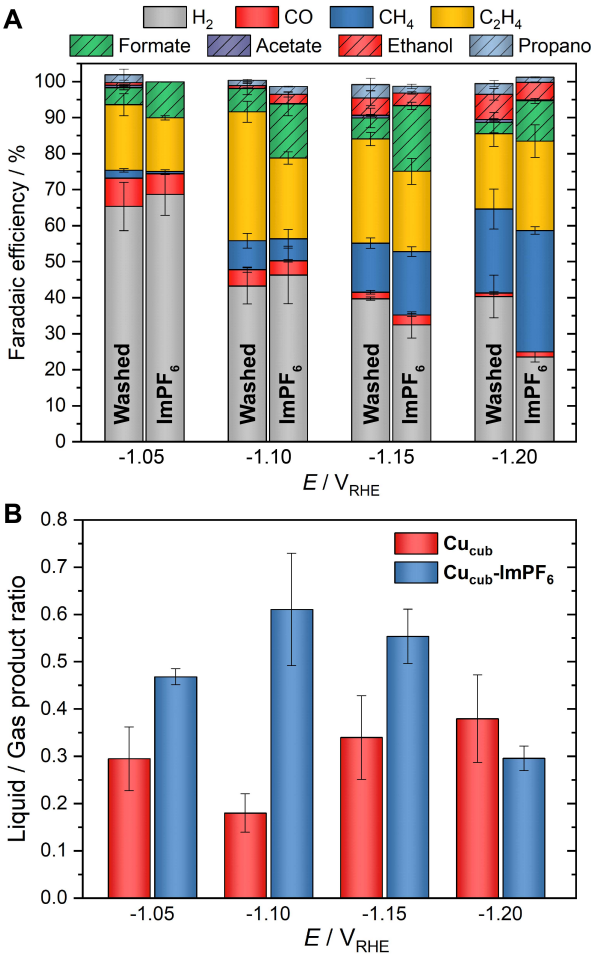


**Figure 3.** A) Faradaic efficiencies for gas and liquid products and (B) liquid/gas product ratios for **$Cu_{cub}$** and **$Cu_{cub}$-$ImPF_6$** measured at different potentials vs the reversible hydrogen electrode (RHE). $CO_2$RR electrolysis was carried out in a liquid H-cell for 75 minutes, using 0.1 M $KHCO_3$ as the electrolyte. The mass loading was 15 µg based on Cu in all cases. Error bars show the standard deviation following three independent measurements. The F.E. values for individual products are given in **Table S2** and shown in **Figure S7**.

While the F.E.s provide a clear idea of product distribution, information regarding changes of the intrinsic catalytic activity can be derived only from current densities normalized by the electrochemically active surface areas (ECSAs). Similar ECSAs were measured for both **$Cu_{cub}$** and **$Cu_{cub}$-$ImPF_6$** ($S_{ECSA}$ = 5.7 $cm^2$, **Figure S8**) indicating that the functionalized CuNCs still retain a large number of free active sites for $CO_2$RR or that perhaps new ones are created post-functionalization. As for the overall current densities for **$Cu_{cub}$** and **$Cu_{cub}$-$ImPF_6$** (**Figure 4A**), they were very similar across the entire potential window studied, thus showing that functionalization with **$ImPF_6$** neither boosts nor inhibits the overall intrinsic activity of the CuNC catalyst towards the $CO_2$RR. Inspection of the partial current densities for the different products reinforces the above-mentioned observations. Namely, they indicate that on **$Cu_{cub}$-$ImPF_6$**, the intrinsic activity for hydrogen is suppressed at higher overpotential (**Figure 4B**); the activity for ethylene decreases at −1.10 and −1.15 $V_{RHE}$ but remains practically unchanged at −1.20 $V_{RHE}$ (**Figure 4C**). Finally, the intrinsic activity for formate is enhanced across the entire potential range (**Figure 4D**).

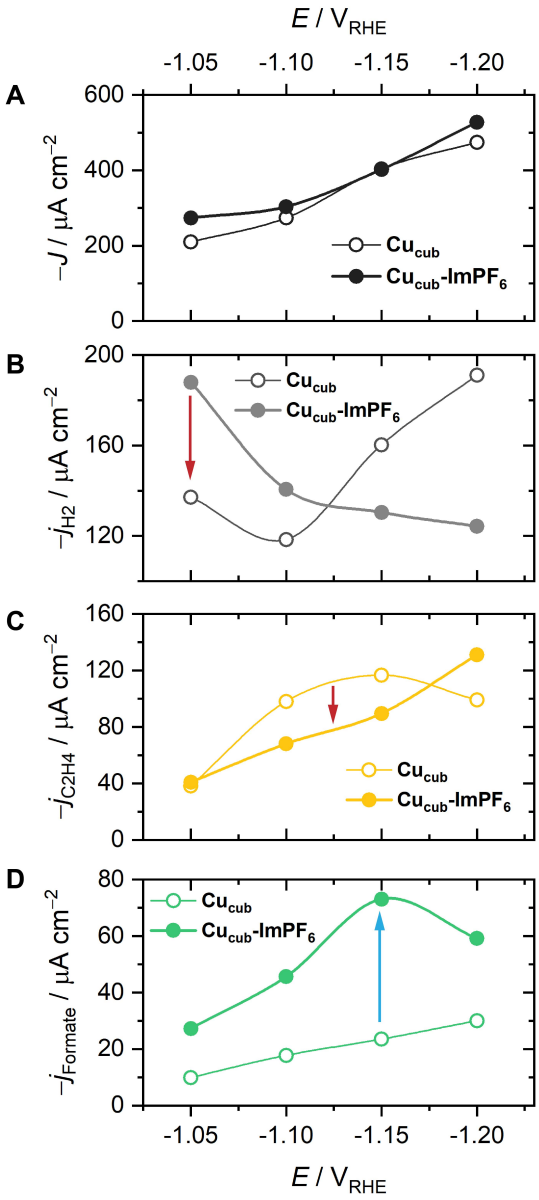


**Figure 4.** A) Total current densities (B) partial current densities for $H_2$ (C) partial current densities for ethylene and (D) partial current densities for formate, for **$Cu_{cub}$** and **$Cu_{cub}$-$ImPF_6$** measured at different potentials vs the reversible hydrogen electrode (RHE). Suppression effects are indicated by a red arrow, while promotion effects are indicated by a blue arrow. $CO_2$RR electrolysis was carried out in a liquid H-cell for 75 minutes, using 0.1 M $KHCO_3$ as the electrolyte.

The mass loading was 15 μg based on Cu in all cases. The partial current densities corresponding to the other products are reported in **Figure S9**.

To explain the discussed changes in selectivity and intrinsic activity due to the presence of **$ImPF_6$** on the Cu surface, we should consider three main roles that ligands can play on the NC surface at the very least. Firstly, ligands can influence the electronic structure of the metal; this was already excluded by XPS measurements, as discussed above. The other possible roles are to influence the metal/electrolyte interface and to interact with incoming reactants or intermediates at the surface.[17]

Ionic liquids have classically been attributed to interacting strongly with $CO_2$,[36] which would result in an increase of local $CO_2$ concentration in the context of our functionalized catalyst. Higher surface hydrophobicity has also been demonstrated to promote the $CO_2$RR vs HER[30,33]; our functionalized catalyst displayed slightly higher hydrophobicity compared with **$Cu_{cub}$** due to the presence of the octyl trail group in **$ImPF_6$** (**Figure S10**). In our system, the presence of the imidazolium ring in **$ImPF_6$** together with the slight increase in hydrophobicity for **$Cu_{cub}$-$ImPF_6$** compared to washed **$Cu_{cub}$** might contribute to the observed increase of $CO_2$RR vs HER activity at higher potential, as we commented in our previous work.[33] To explain the change in selectivity from ethylene to formate is more challenging. In the absence of comprehensive mechanistic studies combined with theory, only speculations can be made for now. Overall, we suspect a convolution of multiple ligand effects at the surface. In addition to those mentioned above, we should also consider the stabilization or trapping of intermediates.[36–38] It is interesting to note that a recent study by Etzold et al. showed that the functionalization of a copper foam with ionic liquid ligands resulted in the suppression of ethylene formation and promotion of liquid products, being mainly formate.[38] This behavior was indeed attributed to the interaction of the ionic liquid ligands with the reaction intermediates, specifically the trapping of the $*CH_2$ carbene.[38]

Suppression of ethylene formation after functionalization of the **$Cu_{cub}$** catalyst is particularly interesting as ethylene should be the main product from the (100) facet of the cubic CuNCs. One of the strengths of colloidal synthesis is the accessibility of preparing NCs with different shapes, which expose different crystal facets on the surface. We took advantage of this to explore the possibility of facet-dependence of the reaction pathway for functionalized CuNCs. Spherical CuNCs (24 nm) were synthesized and were also functionalized with **$ImPF_6$**, which are referred to as **$Cu_{sph}$** and **$Cu_{sph}$-$ImPF_6$**, respectively. The same ligand-exchange procedure was employed as for **$Cu_{cub}$**, and similar characterizing data were obtained that supported the successful ligand exchange (**Figures S11–S13**, **Table S3**). Surprisingly, after functionalization with **$ImPF_6$**, we found that the $CO_2$RR product ratio remained essentially unchanged in the case of the spheres (**Figure S14**). Therefore, we moved on to study the persistence of the ligands on the surface during the $CO_2$RR at −1.1 $V_{RHE}$. **Figure 5** provides an overview of these results.

XPS measurements after $CO_2$RR electrolysis confirmed that the imidazolium ligand is still present on the surface of **$Cu_{Cub}$**, as N1s peaks were observed at 400 and 404 eV that can be ascribed to the imidazolium ring and nitro group of **$ImPF_6$**, respectively (**Figure 5A**). In contrast, these peaks were not observed in the case of **$Cu_{sph}$** (**Figure 5B**). Furthermore, during linear-sweep voltammetry (LSV) measurements, a reduction wave at −0.32 $V_{RHE}$ was observed for **$Cu_{sph}$-$ImPF_6$**. This signature is consistent with ligand stripping[39] and thus indicates that the **$ImPF_6$** ligand readily desorbs from the spherical CuNCs (**Figure 5D**). No such desorption wave was observed for **$Cu_{cub}$-$ImPF_6$** (**Figure 5C**). Effects related to preferential interactions of **$ImPF_6$** with certain facets of the CuNCs (i.e. stronger binding to the (100) surface of the cubic CuNCs) are possible and might play a role here.

In order to assess the structural stability of the inorganic component, we then moved to TEM. Consistent with previous studies on cubic CuNCs[40,41], the **$Cu_{cub}$-$ImPF_6$** catalyst remains stable against restructuring, meaning that they do not change size or shape over the 75 minutes of electrolysis considered in this study (**Figure 5E**). In contrast, **$Cu_{sph}$-$ImPF_6$** converts into larger aggregates containing particles of different sizes and shapes, including some cubic particles (**Figures 5F**, **S15**). Spherical CuNCs are known to undergo immediate restructuring when reductive potentials are applied and we have recently demonstrated that an Ostwald-ripening-like mechanism is involved in such reconstructive processes which start at potentials as low as –0.25 $V_{RHE}$.[11,42,43]

Considering the above observations, we can conclude that the **$Cu_{sph}$-$ImPF_6$** catalyst is unstable at potentials as low as −0.3 $V_{RHE}$, where a combination of potential-induced ligand stripping and change of NC morphology takes place. We highlight that this latter point poses a more general implication for functionalized metal catalysts, where ligands can be "ejected" from a catalyst surface along with the surface atoms during restructuring (**Figure 5G**). A recent study has reported that ligand desorption can be reversible under those unique conditions, including the assembly of NC monolayers on the electrode surface, enabling collective dissociation of ligands under applied bias.[32] This phenomenon is certainly interesting and deserves further investigation. However, we do not observe any immediate evidence for it (e.g. ligand-induced changes in the $CO_2$RR performance of the spherical CuNCs) under the high loading densities utilized in our study.

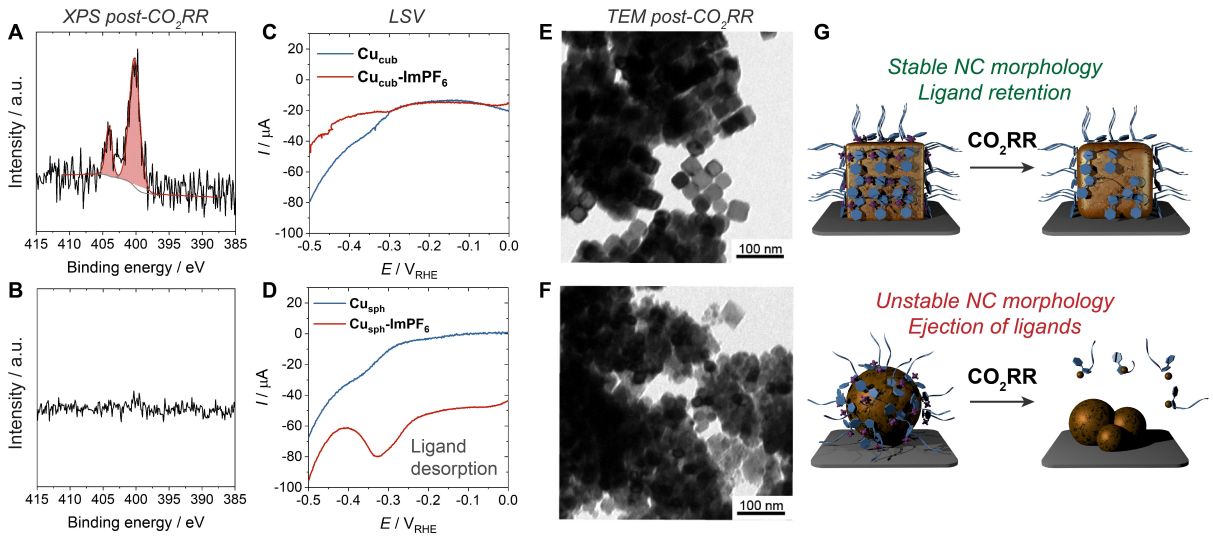


**Figure 5.** A,B) N1s XPS analysis of **$Cu_{cub}$-ImPF$_6$** and **$Cu_{sph}$-ImPF$_6$**, respectively, following $CO_2$RR electrolysis at −1.1 $V_{RHE}$. C,D) LSV of **$Cu_{cub}$-ImPF$_6$** and **$Cu_{sph}$-ImPF$_6$**, respectively. E,F) TEM analysis of **$Cu_{cub}$-ImPF$_6$** and **$Cu_{sph}$-ImPF$_6$**, respectively, following $CO_2$RR electrolysis at −1.1 $V_{RHE}$. G) Scheme depicting the relative stabilities of cubic and spherical CuNCs during the $CO_2$RR.

Finally, another strength of using colloidal NCs as electrocatalysts is that they can be prepared as inks, which facilitates their implementation into different device configurations.[6,15,44] In order to verify whether ligand effects still hold at higher current densities, which are more relevant for commercial applications, we tested **$Cu_{cub}$** and **$Cu_{cub}$-ImPF$_6$** in a gas-fed cell at 50 mA cm$^{-2}$ (**Figure 6**). Both catalysts formed stable colloidal inks that could be sprayed onto carbon paper electrodes. Compared to the measurements in the H-cell, lower overpotentials are needed and suppression of the reactions that form $CH_4$ and $H_2$ are observed, which are changes connected to the reaction microenvironment created in the gas-diffusion electrode and are normally attributed to higher local pH.[6] In terms of $CO_2$RR product selectivity, the same key observations that were made in the liquid H-cell were also made in the gas-fed cell after functionalization with **ImPF$_6$**

(**Figure 6**). Specifically, the ethylene selectivity was reduced from 40.1% to 29.3%, while the F.E. for formate increased from 6.1% to 9.9%. The F.E. for ethanol also increased from 0% to 2.16%, as did that for ethylene glycol, from 0.2% to 2.83%. Overall, the liquid/gas product ratio increased from 0.15 for **$Cu_{cub}$**, to 0.31 for **$Cu_{cub}$-$ImPF_6$**, reflecting the same change in selectivity that was observed in the liquid H-cell.

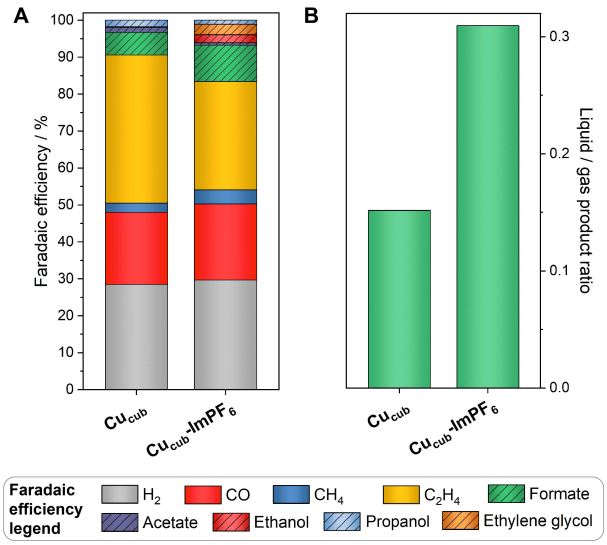


**Figure 6.** Summary of $CO_2$RR selectivity data for **$Cu_{cub}$** and **$Cu_{cub}$-$ImPF_6$**, showing (A) Faradaic efficiencies for gas and liquid products and (B) liquid/gas product ratios. $CO_2$RR electrolysis was carried out in a gas-fed cell for 50 minutes, using 1.2 M $KHCO_3$ as the electrolyte and a fixed current density of −50 mA $cm^{-2}$. The mass loading was 250 μg based on Cu in all cases.

## CONCLUSIONS

In conclusion, we have synthesized hybrid $CO_2$RR catalysts, comprised of inorganic CuNCs functionalized with an imidazolium ligand. The results of our $CO_2$RR studies on cubic CuNCs hint towards the **ImPF$_6$** ligand interacting with $CO_2$ and $CO_2$RR intermediates to promote the $CO_2$RR vs HER at higher applied potentials and formate over ethylene across the entire range of investigated potentials (from −1.05 to −1.20 $V_{RHE}$). After comparing the $CO_2$RR performances of cubic and spherical hybrid CuNCs we have identified that the structural stability of the cubic CuNCs and the stability of their bonds with the ligands permits such surface modification studies. In contrast, the reconstruction of spherical CuNCs means that the promoter effect of the imidazolium ligand is lost. These results point towards the need to design hybrid catalysts with stable NC morphologies in mind or perhaps to conceive ligands that prevent reconstruction processes from occurring. Finally, we would like to highlight that the transferability of a surface-modified NC electrocatalyst from a liquid H-cell into a gas-fed cell is highly encouraging for the future development of such catalysts in the application of the $CO_2$RR.

## ASSOCIATED CONTENT

The Supporting Information is available and free of charge and contains additional experimental details, information related to FT-IR, NMR, XPS, contact angle, electrocatalysis, and TEM results.

## AUTHOR INFORMATION

### Corresponding Author

*Correspondence should be addressed to Prof. Raffaella Buonsanti (raffaella.buonsanti@epfl.ch)

### Author Contributions

The manuscript was written through contributions of all authors. All authors have given approval to the final version of the manuscript.

## ACKNOWLEDGMENT

This work was primarily financed by the H2020 Marie Curie Individual Fellowship grant SURFCAT with agreement number 837378. VO and PY acknowledge the Swiss National Science Foundation (SNSF) under AP Energy Grant, project number PYAPP2_166897/1 and Gaznat SA for financial support. The authors thank Dr. Anna Loiudice for her help with the contact angle measurements.

## ABBREVIATIONS

TOPO, trioctylphosphine oxide; **ImPF$_6$**, 1-octyl-3-(*para*-nitrobenzyl)-imidazolium hexafluorophosphate.

## REFERENCES

(1) Service, R. F. Renewable Bonds. *Science* **2019**, *365*, 1236–1239.
(2) Nitopi, S.; Bertheussen, E.; Scott, S. B.; Liu, X.; Engstfeld, A. K.; Horch, S.; Seger, B.; Stephens, I. E. L.; Chan, K.; Hahn, C.; Nørskov, J. K.; Jaramillo, T. F.; Chorkendorff, I. Progress and Perspectives of Electrochemical $CO_2$ Reduction on Copper in Aqueous Electrolyte. *Chem. Rev.* **2019**, *119*, 7610–7672.
(3) Gao, D.; Arán-Ais, R. M.; Jeon, H. S.; Roldan Cuenya, B. Rational Catalyst and Electrolyte Design for $CO_2$ Electroreduction towards Multicarbon Products. *Nat. Catal.* **2019**, *2*, 198–210.
(4) Huang, J.; Buonsanti, R. Colloidal Nanocrystals as Heterogeneous Catalysts for Electrochemical $CO_2$ Conversion. *Chem. Mater.* **2019**, *31*, 13–25.
(5) Iyengar, P.; Huang, J.; De Gregorio, G. L.; Gadiyar, C.; Buonsanti, R. Size Dependent Selectivity of Cu Nano-Octahedra Catalysts for the Electrochemical Reduction of $CO_2$ to $CH_4$. *Chem. Commun.* **2019**, *55*, 8796–8799.
(6) De Gregorio, G. L.; Burdyny, T.; Loiudice, A.; Iyengar, P.; Smith, W. A.; Buonsanti, R. Facet-Dependent Selectivity of Cu Catalysts in Electrochemical $CO_2$ Reduction at Commercially Viable Current Densities. *ACS Catal.* **2020**, *10*, 4854–4862.
(7) Strasser, P.; Gliech, M.; Kuehl, S.; Moeller, T. Electrochemical Processes on Solid Shaped Nanoparticles with Defined Facets. *Chem. Soc. Rev.* **2018**, *47*, 715–735.

(8) Reske, R.; Mistry, H.; Behafarid, F.; Roldan Cuenya, B.; Strasser, P. Particle Size Effects in the Catalytic Electroreduction of $CO_2$ on Cu Nanoparticles. *J. Am. Chem. Soc.* **2014**, *136*, 6978–6986.
(9) Manthiram, K.; Beberwyck, B. J.; Alivisatos, A. P. Enhanced Electrochemical Methanation of Carbon Dioxide with a Dispersible Nanoscale Copper Catalyst. *J. Am. Chem. Soc.* **2014**, *136*, 13319–13325.
(10) Loiudice, A.; Lobaccaro, P.; Kamali, E. A.; Thao, T.; Huang, B. H.; Ager, J. W.; Buonsanti, R. Tailoring Copper Nanocrystals towards $C_2$ Products in Electrochemical $CO_2$ Reduction. *Angew. Chem. Int. Ed.* **2016**, *55*, 5789–5792.
(11) Kim, D.; Kley, C. S.; Li, Y.; Yang, P. Copper Nanoparticle Ensembles for Selective Electroreduction of $CO_2$ to $C_2$ –$C_3$ Products. *Proc. Natl. Acad. Sci.* **2017**, *114*, 10560–10565.
(12) Osowiecki, W. T.; Nussbaum, J. J.; Kamat, G. A.; Katsoukis, G.; Ledendecker, M.; Frei, H.; Bell, A. T.; Alivisatos, A. P. Factors and Dynamics of Cu Nanocrystal Reconstruction under $CO_2$ Reduction. *ACS Appl. Energy Mater.* **2019**, *2*, 7744–7749.
(13) Mangione, G.; Huang, J.; Buonsanti, R.; Corminboeuf, C. Dual-Facet Mechanism in Copper Nanocubes for Electrochemical $CO_2$ Reduction into Ethylene. *J. Phys. Chem. Lett.* **2019**, *10*, 4259–4265.
(14) Zhu, P.; Xia, C.; Liu, C.-Y.; Jiang, K.; Gao, G.; Zhang, X.; Xia, Y.; Lei, Y.; Alshareef, H. N.; Senftle, T. P.; Wang, H. Direct and Continuous Generation of Pure Acetic Acid Solutions via Electrocatalytic Carbon Monoxide Reduction. *Proc. Natl. Acad. Sci.* **2021**, *118*, e2010868118.
(15) Wang, Y.; Shen, H.; Livi, K. J. T.; Raciti, D.; Zong, H.; Gregg, J.; Onadeko, M.; Wan, Y.; Watson, A.; Wang, C. Copper Nanocubes for $CO_2$ Reduction in Gas Diffusion Electrodes. *Nano Lett.* **2019**, *19*, 8461–8468.
(16) Dunfeng, G.; Zegkinoglou, I.; Divins, N. J.; Scholten, F.; Sinev, I.; Grosse, P.; Roldan Cuenya, B. Plasma-Activated Copper Nanocube Catalysts for Efficient Carbon Dioxide Electroreduction to Hydrocarbons and Alcohols. *ACS Nano* **2017**, *11*, 4825–4831.
(17) Ung, D.; Murphy, I. A.; Cossairt, B. M. Designing Nanoparticle Interfaces for Inner-Sphere Catalysis. *Dalton Trans.* **2020**, *49*, 4995–5005.
(18) Rossi, L. M.; Fiorio, J. L.; Garcia, M. A. S.; Ferraz, C. P. The Role and Fate of Capping Ligands in Colloidally Prepared Metal Nanoparticle Catalysts. *Dalton Trans.* **2018**, *47*, 5889–5915.
(19) Li, J.; Zhang, Y.; Kornienko, N. Heterogeneous Electrocatalytic Reduction of $CO_2$ Promoted by Secondary Coordination Sphere Effects. *New J. Chem.* **2020**, *44*, 4246–4252.
(20) Franco, F.; Rettenmaier, C.; Jeon, H. S.; Roldan Cuenya, B. Transition Metal-Based Catalysts for the Electrochemical $CO_2$ Reduction: From Atoms and Molecules to Nanostructured Materials. *Chem. Soc. Rev.* **2020**, *49*, 6884–6946.
(21) Wagner, A.; Sahm, C. D.; Reisner, E. Towards Molecular Understanding of Local Chemical Environment Effects in Electro- and Photocatalytic $CO_2$ Reduction. *Nat. Catal.* **2020**, *3*, 775–786.
(22) Nam, D.-H.; De Luna, P.; Rosas-Hernández, A.; Thevenon, A.; Li, F.; Agapie, T.; Peters, J. C.; Shekhah, O.; Eddaoudi, M.; Sargent, E. H. Molecular Enhancement of Heterogeneous $CO_2$ Reduction. *Nat. Mater.* **2020**, *19*, 266–276.
(23) Cao, Z.; Kim, D.; Hong, D.; Yu, Y.; Xu, J.; Lin, S.; Wen, X.; Nichols, E. M.; Jeong, K.; Reimer, J. A.; Yang, P.; Chang, C. J. A Molecular Surface Functionalization Approach to

Tuning Nanoparticle Electrocatalysts for Carbon Dioxide Reduction. *J. Am. Chem. Soc.* **2016**, *138*, 8120–8125.

(24) Cao, Z.; Derrick, J. S.; Xu, J.; Gao, R.; Gong, M.; Nichols, E. M.; Smith, P. T.; Liu, X.; Wen, X.; Copéret, C.; Chang, C. J. Chelating N-Heterocyclic Carbene Ligands Enable Tuning of Electrocatalytic $CO_2$ Reduction to Formate and Carbon Monoxide: Surface Organometallic Chemistry. *Angew. Chem. Int. Ed.* **2018**, *57*, 4981–4985.

(25) Li, F.; Thevenon, A.; Rosas-Hernández, A.; Wang, Z.; Li, Y.; Gabardo, C. M.; Ozden, A.; Dinh, C. T.; Li, J.; Wang, Y.; Edwards, J. P.; Xu, Y.; McCallum, C.; Tao, L.; Liang, Z.-Q.; Luo, M.; Wang, X.; Li, H.; O'Brien, C. P.; Tan, C.-S.; Nam, D.-H.; Quintero-Bermudez, R.; Zhuang, T.-T.; Li, Y. C.; Han, Z.; Britt, R. D.; Sinton, D.; Agapie, T.; Peters, J. C.; Sargent, E. H. Molecular Tuning of $CO_2$-to-Ethylene Conversion. *Nature* **2020**, *577*, 509–513.

(26) Ahn, S.; Klyukin, K.; Wakeham, R. J.; Rudd, J. A.; Lewis, A. R.; Alexander, S.; Carla, F.; Alexandrov, V.; Andreoli, E. Poly-Amide Modified Copper Foam Electrodes for Enhanced Electrochemical Reduction of Carbon Dioxide. *ACS Catal.* **2018**, *8*, 4132–4142.

(27) Wang, Z.; Wu, L.; Sun, K.; Chen, T.; Jiang, Z.; Cheng, T.; Goddard, W. A. Surface Ligand Promotion of Carbon Dioxide Reduction through Stabilizing Chemisorbed Reactive Intermediates. *J. Phys. Chem. Lett.* **2018**, *9*, 3057–3061.

(28) Wang, Z.; Sun, K.; Liang, C.; Wu, L.; Niu, Z.; Gao, J. Synergistic Chemisorbing and Electronic Effects for Efficient $CO_2$ Reduction Using Cysteamine-Functionalized Gold Nanoparticles. *ACS Appl. Energy Mater.* **2019**, *2*, 192–195.

(29) Fang, Y.; Flake, J. C. Electrochemical Reduction of $CO_2$ at Functionalized Au Electrodes. *J. Am. Chem. Soc.* **2017**, *139*, 3399–3405.

(30) Buckley, A. K.; Lee, M.; Cheng, T.; Kazantsev, R. V.; Larson, D. M.; Goddard III, W. A.; Toste, F. D.; Toma, F. M. Electrocatalysis at Organic–Metal Interfaces: Identification of Structure–Reactivity Relationships for $CO_2$ Reduction at Modified Cu Surfaces. *J. Am. Chem. Soc.* **2019**, *141*, 7355–7364.

(31) Wakerley, D.; Lamaison, S.; Ozanam, F.; Menguy, N.; Mercier, D.; Marcus, P.; Fontecave, M.; Mougel, V. Bio-Inspired Hydrophobicity Promotes $CO_2$ Reduction on a Cu Surface. *Nat. Mater.* **2019**, *18*, 1222–1227.

(32) Kim, D.; Yu, S.; Zheng, F.; Roh, I.; Li, Y.; Louisia, S.; Qi, Z.; Somorjai, G. A.; Frei, H.; Wang, L.-W.; Yang, P. Selective $CO_2$ Electrocatalysis at the Pseudocapacitive Nanoparticle/Ordered-Ligand Interlayer. *Nat. Energy* **2020**, *5*, 1032–1042.

(33) Pankhurst, J. R.; Guntern, Y. T.; Mensi, M.; Buonsanti, R. Molecular Tunability of Surface-Functionalized Metal Nanocrystals for Selective Electrochemical $CO_2$ Reduction. *Chem. Sci.* **2019**, *10*, 10356–10365.

(34) Thevenon, A.; Rosas-Hernández, A.; Peters, J. C.; Agapie, T. In-Situ Nanostructuring and Stabilization of Polycrystalline Copper by an Organic Salt Additive Promotes Electrocatalytic $CO_2$ Reduction to Ethylene. *Angew. Chem. Int. Ed.* **2019**, *58*, 16952–16958.

(35) Kuhl, K. P.; Cave, E. R.; Abram, D. N.; Jaramillo, T. F. New Insights into the Electrochemical Reduction of Carbon Dioxide on Metallic Copper Surfaces. *Energy Environ. Sci.* **2012**, *5*, 7050.

(36) Rosen, B. A.; Salehi-Khojin, A.; Thorson, M. R.; Zhu, W.; Whipple, D. T.; Kenis, P. J. A.; Masel, R. I. Ionic Liquid-Mediated Selective Conversion of $CO_2$ to CO at Low Overpotentials. *Science* **2011**, *334*, 643–644.

(37) Lau, G. P. S.; Schreier, M.; Vasilyev, D.; Scopelliti, R.; Grätzel, M.; Dyson, P. J. New Insights Into the Role of Imidazolium-Based Promoters for the Electroreduction of $CO_2$ on a Silver Electrode. *J. Am. Chem. Soc.* **2016**, *138*, 7820–7823.
(38) Zhang, G.; Straub, S.; Shen, L.; Hermans, Y.; Schmatz, P.; Reichert, A. M.; Hofmann, J. P.; Katsounaros, I.; Etzold, B. J. M. Probing $CO_2$ Reduction Pathways for Copper Catalysis Using an Ionic Liquid as a Chemical Trapping Agent. *Angew. Chem. Int. Ed.* **2020**, *59*, 18095–18102.
(39) Pankhurst, J. R.; Iyengar, P.; Loiudice, A.; Mensi, M.; Buonsanti, R. Metal–Ligand Bond Strength Determines the Fate of Organic Ligands on the Catalyst Surface during the Electrochemical $CO_2$ Reduction Reaction. *Chem. Sci.* **2020**, *11*, 9296–9302.
(40) Huang, J.; Hörmann, N.; Oveisi, E.; Loiudice, A.; De Gregorio, G. L.; Andreussi, O.; Marzari, N.; Buonsanti, R. Potential-Induced Nanoclustering of Metallic Catalysts during Electrochemical $CO_2$ Reduction. *Nat. Commun.* **2018**, *9*, 3117.
(41) Grosse, P.; Gao, D.; Scholten, F.; Sinev, I.; Mistry, H.; Roldan Cuenya, B. Dynamic Changes in the Structure, Chemical State and Catalytic Selectivity of Cu Nanocubes during $CO_2$ Electroreduction: Size and Support Effects. *Angew. Chem. Int. Ed.* **2018**, *57*, 6192–6197.
(42) Vavra, J.; Shen, T.; Stoian, D.; Tileli, V.; Buonsanti, R. Real-time Monitoring Reveals Dissolution/Redeposition Mechanism in Copper Nanocatalysts during the Initial Stages of the $CO_2$ Reduction Reaction. *Angew. Chem. Int. Ed.* **2021**, *60*, 1347–1354.
(43) Li, Y.; Kim, D.; Louisia, S.; Xie, C.; Kong, Q.; Yu, S.; Lin, T.; Aloni, S.; Fakra, S. C.; Yang, P. Electrochemically Scrambled Nanocrystals Are Catalytically Active for $CO_2$-to-Multicarbons. *Proc. Natl. Acad. Sci.* **2020**, *117*, 9194–9201.
(44) Möller, T.; Scholten, F.; Thanh, T. N.; Sinev, I.; Timoshenko, J.; Wang, X.; Jovanov, Z.; Gliech, M.; Roldan Cuenya, B.; Varela, A. S.; Strasser, P. Electrocatalytic $CO_2$ Reduction on $CuO_x$ Nanocubes: Tracking the Evolution of Chemical State, Geometric Structure, and Catalytic Selectivity Using Operando Spectroscopy. *Angew. Chem. Int. Ed.* **2020**, *59*, 17974–17983.